



HAL
open science

Influence of chemical composition on the microstructure and phase transformations of Fe-14Cr ferritic steels

Mickaël Dadé, Joel Malaplate, Jean-Christophe C Brachet, Thomas Guilbert, Caroline Toffolon

► **To cite this version:**

Mickaël Dadé, Joel Malaplate, Jean-Christophe C Brachet, Thomas Guilbert, Caroline Toffolon. Influence of chemical composition on the microstructure and phase transformations of Fe-14Cr ferritic steels. *Materialia*, 2019, pp.100388. 10.1016/j.mtla.2019.100388 . cea-03238498

HAL Id: cea-03238498

<https://cea.hal.science/cea-03238498>

Submitted on 27 May 2021

HAL is a multi-disciplinary open access archive for the deposit and dissemination of scientific research documents, whether they are published or not. The documents may come from teaching and research institutions in France or abroad, or from public or private research centers.

L'archive ouverte pluridisciplinaire **HAL**, est destinée au dépôt et à la diffusion de documents scientifiques de niveau recherche, publiés ou non, émanant des établissements d'enseignement et de recherche français ou étrangers, des laboratoires publics ou privés.



Distributed under a Creative Commons Attribution - NonCommercial - NoDerivatives 4.0 International License

Influence of chemical composition on the microstructure and phase transformations of Fe-14Cr ferritic steels

M. Dadé^{a,*1}, J. Malaplate^a, J.C. Brachet^a, T. Guilbert^a, C. Toffolon-Masclét^a

^a DEN-Service de Recherches Métallurgiques Appliquées, CEA, Université Paris-Saclay, F-91191 Gif-Sur-Yvette, France

* Corresponding author E-mail address : mickael.dade@eramet.com

¹ Present address: ERAMET IDEas, 1 avenue Albert Einstein, 78190, Trappes, France

ABSTRACT

The effect of strengthened elements (Y_2O_3 and TiO_2) on the microstructure has been investigated in Fe-14Cr-1W based ferritic steels. Titanium content and/or volume fraction of yttria range between ~ 0 up to 0.3 wt%.

The volume fraction of nanoparticles is shown to control the grain size whereas titanium content has a significant influence on the chemical homogeneity. Martensite phase was obtained on a Fe-14Cr-1W based ferritic steel after consolidation by Hot Isostatic Pressing because of a higher content of carbon. A relationship between martensite phase and chemical heterogeneities was evidenced showing a chemical partitioning phenomenon. This phenomenon was also observed on ODS ferritic steels containing a low content of titanium (≤ 0.05 wt%) however microstructural parameters, such as size and volume fraction of nano-precipitates and grain size, are shown to delay the formation of martensite during cooling by decreasing the value of critical cooling rate.

Thermodynamic calculations indicate that the minimal titanium content to get a microstructure with 100% of ferrite is about 0.09 wt%.

Keywords: ODS ferritic steel, Chemical heterogeneities, Partitioning, Martensite

1. INTRODUCTION

For the next generation of nuclear reactors (GEN IV), Oxide Dispersion Strengthened (ODS) ferritic/martensitic steels are studied as potential materials for nuclear fuel cladding application. They have been studied over the last decades owing to their good mechanical properties (i.e., in particular improvement of high temperature creep properties due to structural hardening by an adequate oxide dispersion) and their excellent resistance to swelling under irradiation [1-3].

The prime requirement for the performance of ODS steels is to obtain a distribution of nanometer-size oxide particles homogeneously distributed inside the matrix. ODS ferritic/martensitic steels are thus usually elaborated by powder metallurgy. A pre-alloyed powder, previously atomized, is milled with yttria powder (Y_2O_3) using a high-energy attritor under a protective atmosphere.

Atom Probe Tomography (APT) and Small-Angle Scattering (SAS) investigations have shown that Y, Ti and O are dissolved, at least partially, and driven in solid solution during high-energy ball milling [4-6]. Finally, the mixed powder is canned and consolidated by Hot Extrusion (HE) or Hot Isostatic Pressing (HIP) [7-8]. Recently, Spark Plasma Sintering (SPS) processes have been used to consolidate the milled powder in several studies [9-10].

The microstructure of ferritic/martensitic steels strongly depends on these consolidation processes [11-12] but also on the chemical composition [13-14]. The combination of powder metallurgy process route with the presence of a dispersion of nano-oxide results in a very small grain size, partly sub-micrometric [13, 15]. The grain size distribution is frequently bi-modal, due to complex abnormal grain growth mechanisms [16]. Furthermore, as illustrated by Al-Mangour in Fig. 1 [17], low chromium content (< 12 wt%) steels present a phase transformation $\alpha \rightarrow \gamma$ above about 850°C . An understanding of the physical metallurgy of low activation 7-11%Cr martensitic steels have been carried out by Alamo et al. [18] to optimize the microstructure and thus the mechanical properties. Moreover, Brachet et al. [19] shows that the critical cooling rate values for martensite/ferrite occurrence depends on the prior austenitic grain size, which is also correlated to the addition of nano-particles. A lower prior austenitic grain diameter induces a higher critical cooling rate value.

As illustrated in Fig. 1, there is no phase transformation at high temperature for steels with chromium content above 13 wt%; only ferritic steels are obtained [20]. Due to the high content of chromium, the corrosion and oxidation resistance of ferritic steels are improved compared to lower chromium containing martensitic steels [21]. In recent studies, martensitic microstructure has been observed in Fe-14%Cr steels consolidated by HIP without powder metallurgy process route (high energy milling) [13,22]. Nevertheless, the occurrence of this martensitic microstructure is still unclear.

In this context, the aim of the present work is to study the phase transformations of un-strengthened Fe-14Cr ferritic steels and compare with several ODS ferritic steels to understand the effect of the nano-particles addition on the occurrence, or not, of cooling martensitic phase transformation. For the different re-inforced ferritic steels studied here, different contents of titanium and/or yttria have been introduced to study the effect of strengthening

element on the microstructure. In order to avoid the complex microstructure obtained by hot extrusion (elongated grains, nano-particles, high dislocations density, crystallographic texture) [23-24], every material has been consolidated by Hot Isostatic Pressing (HIP). They are all based on the same matrix chemical composition, with 14%Cr and 1%W. The volume fraction and size of oxide particles have been monitored by adding different amounts of Y and Ti.

The microstructure of these different materials has been characterized by a combination of different experimental technics. The grain size and morphology have been evaluated by Scanning Electron Microscopy (SEM) coupled with Electron BackScatter Diffraction (EBSD) analyses. Electron Probe Micro Analyzer (EPMA) has been carried out for chemical analyses. Then, the phase transformations have been studied by dilatometry (DIL) and calorimetry (CALO).

2. MATERIALS AND METHODS

Fe-14Cr ferritic steels re-inforced by a fine oxide dispersion were produced by mechanical alloying. The mixture contains a pre-alloyed powder and Y_2O_3 and/or TiH_2 powders. A Union Process SD01 attritor has been used for ball milling under argon atmosphere for 10 h. The ball-to-powder ratio was 15:1. In order to avoid any contaminations of Y or Ti for the un-strengthened material, the atomized powder was not milled. All powders (ball-milled state or atomized state) were canned and annealed for two hours at intermediate temperature (300 or 400°C depending of the material) to reduce the amount of oxygen. Finally, each materials were consolidated at 1100°C by Hot Isostatic Pressing (HIP) (1900 bars, 2 h).

The compositions (in wt%) of each ferritic steels are given in [Table 1](#). The base alloy composition is the same for every material with approximately 14% Cr and 1% W. Ti and Y content have been adjusted to study the effect of strengthening and contamination elements on the microstructure, and notably on the phase transformation. Four different ferritic steels have been elaborated: an un-strengthened material (**US**) with no addition of Ti and Y, a low strengthened material (**LS**) with a low fraction of Ti and Y_2O_3 , a reference material (**Ref**) with a fraction of oxides typical of most of the ODS types materials studied in the literature and a material based on the **Ref** alloy but without Ti (**WTi**).

The microstructure of all materials were examined with a Field Emission Gun SEM JEOL JSM-7001FLV apparatus with a voltage of 20 kV. Samples were mechanically mirror polished followed by electropolishing, using an electrolyte containing 70% of ethanol, 20% of ethylene glycol monobutyl ether and 10% of perchloric acid, used at 5°C with a tension of 27 V during 30 seconds to allow the EBSD analysis.

Chemical analyses, filiations and concentration maps were performed on a CAMECA SX-100 Electron Probe Micro Analyzer (EPMA).

Dilatometric measurements have been carried out with a modified DT1000 ADAMEL-LHORMARGY apparatus. Rectangular samples (12x2x2 mm³) have been treated with a heating rate of 10°C/s up to the target high temperature and a cooling rate from 0.1°C/s to 100°C/s. Moreover, calorimetric measurements were also performed with a SETARAM-multi-HTC high temperature calorimeter. It enables us to heat samples with a typical mass ~1g until 1400°C under inert gas (argon). The heating rate was 10°C/min whereas the specimens were cooled with a furnace shutted off.

3. RESULTS

3.1. Microstructural characterizations

Figs. 2a and b show the microstructure of **US** and **Ref** ferritic steels for the same magnification. As expected, the grain structures of these two materials are isotropic without crystallographic texture compared to hot extruded materials [12]. These grain structures are also observed for the two other ODS ferritic steels. With or without Ti and Y₂O₃, the microstructure is bimodal for each material. Nevertheless, one can see that the un-strengthened ferritic steel exhibits a microstructure with larger grains (10-50 μm). On the contrary, our previous study [13] has shown that the studied ODS ferritic steels are composed of large grains with a maximal size close to 10 μm and very small grains (100-300 nm), which have been observed at higher magnification. This microstructural difference is likely related to the consolidation method, which has been carried out directly after powder atomization for the **US** material. Moreover, the grain size of **US** steel is higher due to the lack of nano-oxides, which may pin the grain boundaries. As suggested by recent studies [13,22], martensite phase was observed in the **US** material as illustrated Fig. 2c. Then, small grains are observed on ODS ferric steels whereas martensitic blocks replace these small grains for the **US** material.

From EBSD maps realized at different magnifications, the mean grain size and surface fraction of small grains/martensite areas have been estimated. They are given in Table 2. If we compare the **US**, **LS** and **WTi** materials, it is interesting to note that the surface fraction of small grains or martensite blocks increases with the titanium content. It probably explains why the average grain size of **LS** is lower compared to **Ref** material.

Coarse precipitations, located at more or less circular grain boundaries, are also observed in Fig. 2a. Those particular locations should correspond to the initial surface of atomized powders. Furthermore, the diameter is about 80 μm , which is consistent with the average atomized powder size. The precipitation state of each material is given in Table 2. As discussed in [13], the average nano-particles size and their volume fraction have been determined by Small Angle X-Ray Scattering (SAXS) measurements. As expected, the **US** material is free of nano-oxides. Furthermore, the oxides volume fraction of the **LS** ferritic steel is lower than that of the **Ref** material. From the comparison between the ferritic without titanium and the reference material, it appears that the average size of oxides increases and thus the volume fraction decreases when the titanium content decreases. It is in good agreement with Dou et al. results [14].

3.2. Chemical analyses

For every material, chemical analyses have been carried out using EPMA. Fig. 3 shows the EPMA maps for each element analyzed (Cr, W, Ti, Al, O and Y). For all the studied ferritic steels, with or without Ti and Y_2O_3 , localized oxygen enrichments have occurred. These oxygen enrichments present a shape looking like rims of as-milled powder particles for the **WTi**, **Ref** and **LS** materials whereas the oxygen segregations of the **US** material have spherical shape as the former atomized powder particles. A correlation between O, Ti and Al segregations can be noted on the **Ref** and **LS** materials whereas chromium or aluminum oxides are observed for the two other materials without titanium. Filiations of strengthened materials presented in Figs. 4 highlight the fact that these oxygen segregations are located at some precipitation sites, as can be deduced from the observations of punctual maxima. Moreover, the quantitative analyses confirm the association between O and Ti or O and Cr with sometimes some local enrichment in Al.

Despite O, Ti and Al segregations, at the EPMA micrometer scale, a good homogeneity is observed for the **Ref** ferritic steels, especially for the Cr and W EPMA maps. On the contrary, segregations of Cr and W are observed for the **WTi**, **LS** and **US** EPMA maps. W segregations have been observed recently on a martensitic 9Cr ODS steel

after HIP, HE and heat treatment [25]. Moreover, Cr segregations were noticed on a Fe-14Cr based alloy consolidated by hot uniaxial pressing [26]. It is interesting to note that the ratio of Cr- and W-rich areas increases with the titanium content. Indeed, the un-strengthened material is only constituted by 14% depleted zones against 43% and 38% respectively for **LS** and **WTi** ODS steels. The area fractions of Cr- and W-depleted zones have been estimated using an image processing software on EPMA maps. It can also be noticed that the ratio of martensite blocks in the US materials estimated by EBSD analyses (Table 2) is closed to the area fractions of Cr- and W-depleted zones.

A complementary study has been realized with EPMA analyses on the **US** material. Quantitative analyses have been carried out to match segregations of Cr and W observed on the EPMA maps within the matrix. The filiation goes through large grains and martensitic blocks. As illustrated in Fig. 5, a relationship between Cr and W concentrations and grains is highlighted. The large grains are composed of ~ 14.3 wt% Cr and ~ 1 wt% W whereas the concentration of these two elements is lower in martensitic blocks (~ 13 wt% Cr and ~ 0.7 wt% W respectively). The same tendency was observed for the **LS** and **WTi** steels. Indeed, the large grains are associated to the Cr- and W-rich zones. However, it was more difficult to underline the relationship between the depleted areas with the small grains.

In a general manner, segregations of Cr and W have been observed on material containing a small amount or no titanium at all. These segregations suggest the occurrence of chemical partitioning during the thermo-mechanical treatment.

3.3. Phase transformations

To characterize the phase transformations of each model material, dilatometric and calorimetric measurements were carried out. Tests were done under protective atmosphere (argon or helium) to prevent oxidation at high temperature.

Fig. 6a shows the evolution of the relative thermal expansion $\left(\frac{\Delta L}{L_0}\right)$ of the **Ref** ODS ferritic steel with the temperature. The thermal cycle is the following:

- From room temperature to 1100°C with a heating rate of 10°C/s
- Holding at 1100°C for 1 minute

- Cooling from 1100°C to room temperature with a rapid quenching (100°C/s).

Despite this very high cooling rate, it can be seen that there is no inflexion points, corresponding to allotropic phase transformations, which could occur during the heating and the cooling steps. Dilatometric tests have also been carried out on **US** and **LS** materials using the elaboration conditions (heating up to 1100°C with a cooling rate of 0.2°C/s close to HIP conditions). As illustrated in [Figs. 6b](#) and [c](#), martensite is formed for the **US** whereas austenite is transformed into ferrite during cooling for the **LS** material. As highlighted by Brachet et al. [19], this difference could be due to the effect of the prior austenite-grain size.

Calorimetric tests were also carried out and confirm that the **Ref** material presents no phase transformation despite an endothermic and an exothermic peak observed close to 700°C respectively during heating and cooling steps ([Fig. 7](#)). These peaks correspond to the Curie temperature, which is usually observed for ferromagnetic materials [27-28]. During the calorimetric tests, the cooling rate was close to 0.5°C/s, which corresponds to a cooling with a furnace shutted off. However this order of cooling rate should varied during the cooling due to furnace inertia.

On the contrary, the DSC curve of **LS** steel shows a small endothermic inflexion near 880°C during the heating. This endothermic peak is also observed towards 870°C and 840°C respectively for the **WTi** and **US** steels during heating ([Fig. 7a](#)). It likely corresponds to a phase transformation from ferritic phase α to austenitic phase γ . During cooling ([Fig. 7b](#)), **WTi** steel is the only steel which exhibits an exothermic peak at temperature close to 800°C. This peak likely corresponds to the back transformation of austenite into ferrite. Inversely, DSC curves of **US** and **LS** ferritic steels show an exothermic peak at lower temperature (310-330°C) during cooling ([Fig. 7b](#)), which is usually associated to the martensitic transformation. It means that the austenite is transformed into martensite for these two steels. A variation of the onset temperature A_{c1} with Ti and Y_2O_3 contents can be noticed. Defining A_{c1} as the onset temperature and A_{c3} as the end temperature, the DSC plot was used to calculate the enthalpy associated with the ferrite to austenite phase transformation. The phase transformation enthalpy ($\Delta H^{\alpha \rightarrow \gamma}$) was calculated for each material. Furthermore, the ratio of transformed ferrite was determined using enthalpy value of ferrite to austenite transformation of a Fe-9Cr steel [29]. [Table 3](#) gives the calculated enthalpy and austenite content values. For each material, the austenite contents indicate that the phase transformations are not complete during heating. Furthermore, a good agreement between the estimated austenite content and the Cr- and W-depleted areas, and thus with the surface fraction of small grains/martensite blocks can be noticed.

In order to draw the Continuous Cooling Transformations diagram (CCT diagram), several dilatometric tests have been carried out on the **WTi** ferritic steel. Cooling rates applied were ranging between 0.1°C/s and 100°C/s. Fig. 8 shows a partial or complete martensitic transformation when the cooling rate is higher than 0.5°C/s. During the HIP process, the cooling rate was about 0.2°C/s. Dilatometric results show that for this low cooling rate, there is no martensitic transformation, which is in good agreement with the as-received microstructural observations.

As illustrated by dilatometric and calorimetric tests, ferritic steels containing a low or no titanium content exhibit a phase transformation from α to $\alpha + \gamma$ during heating. Thus, this partial austenitization generates chemical partitioning of alloying chemical elements such as Cr and W, explaining the existence of Cr and W segregated areas in the final microstructure.

4. DISCUSSIONS

4.1. Effect of titanium content

In this work, the effect of titanium on the microstructure and the phase transformation have been studied with an ODS Fe-14Cr-1W steel without titanium.

First, titanium, aluminum and oxygen segregations were observed on EPMA maps in ODS Fe-14Cr-1W steel with titanium. It corresponds to coarse precipitation usually observed on ODS ferritic steels [30]. According to Cunat [31], titanium has a higher affinity with oxygen and carbon than chromium. On the contrary, when there is no titanium, Cr-rich particles are formed. As observed by Olier et al. [32] and Auger et al. [20], these large particles could be chromium oxides and/or carbides type $(\text{Fe, Cr})_{23}\text{C}_6$. Concerning the nano-particles, increasing size was observed when titanium content decreases. This effect has been previously observed by Okuda et al. [33] and confirmed by Alinger et al., Kim et al. and Ratti et al. [4, 34-35].

Microstructural results show that an effect of titanium content is anticipated on the phase diagram. Indeed, depleted zones of Cr and W have been observed for the ferritic steels containing an extremely low (or zero) titanium content whereas the **Ref** material shows no segregations of Cr and W. EPMA results highlight the fact that these heterogeneous zones are associated to martensite block for **US** material and small grains for **LS** and **WTi** materials. According to dilatometric and DSC measurements, these three ferritic steels present a chemical partitioning during the HIP process due to the incomplete austenitization leading to a two phase $\alpha + \gamma$ metallurgical state at high temperature. Thus, a part of ferrite is transformed into austenite. Nevertheless, titanium is known to be

an alphagene element [31]. Moreover, Fig. 9a shows the calculated Fe-Cr-W ternary diagram and shows that there is no $\alpha + \gamma$ phase field extending up to 1100°C for a Fe-14Cr-1W ferritic steel. It would mean that these microstructural heterogeneities are due to the gammagene elements such as nitrogen, carbon, nickel or manganese. Table 4 gives the concentration of Ni, N, C and Mn for each model material. Mass contents have been measured by Inductively Coupled Plasma analyses. According to Cunat [31], nickel does not impact the γ phase field of a Fe-17Cr when the concentration is lower than 2%. Chemical analyses show that the average mass content does not exceed 0.22% and thus is not enough to impact the phase transformations. Although considered as a gammagene element, Mn may have limited effect on the phase transformation for the content experienced here. Indeed, it would have no significant influence on the austenitic phase field but may affect the phase transformation kinetics upon cooling [31]. Thus, chemical elements, which may have the strongest influence on the austenitic domain, would be nitrogen and carbon. Fig. 9b indicates that the carbon has an important role on the bimodal $\alpha + \gamma$ domain. Indeed, it is observed that the size of the $\alpha + \gamma$ phase field increases with the carbon content. Mass contents of C vary from 0.01% for the **US** material to 0.03 – 0.05% for the ODS ferritic steels. It means that strengthened ferritic steels may present phase transformations however this is not the case for **Ref** material. It is known that titanium is a strong carbide-forming element [38] which reduces the mass content of carbon in solid solution and thus avoid the phase transformation up to high temperatures. As observed in a recent study [39], the lack of titanium, and thus titanium carbide, would thus explain the appearance of α to $\alpha + \gamma$ transformations during heating of **US** and **WTi** materials. Fig. 10a shows the pseudo-binary phase diagram, calculated by Thermocalc software (TCFE7 database), of **Ref** material with a variation of C content. The titanium content used for this computation is the mass percent of Ti which is not trapped into the nanometric oxides Y-Ti-O. This titanium content was estimated by a mass balance calculation. The red dashed line corresponds to the mass content obtained by quantitative analyses (Table 4). It appears that the **Ref** material crossed the ferritic α domain at high temperatures, which is in good agreement with dilatometric and calorimetric measurements (Figs. 6a and 7). Inversely, a Fe-14Cr-1W without Ti exhibits a restricted α phase domain with the increase of carbon content (Fig. 10b). This C-effect on the phase transformation was suspected by Oka [25] but it was not clearly demonstrated. The pseudo-binary phase diagram shows that **LS** (0.03 wt%) and **WTi** (0.05 wt%) ferritic steels experienced phase transformations upon heating. Then, Fig. 10c gives the evolution of phase transformation with titanium content of a Fe-14Cr-1W-0.3C steel. It can be deduced

from this plot that the lowest titanium content in solid solution to obtain a 100% Fe-14Cr-1W ferritic steel containing 0.3% C, is around 0.09 wt%.

4.2. Effect of nano-oxides addition and volume fraction

Microstructural characterization clearly showed a strong effect of nano-oxides addition on the average grain size. Indeed, without strengthened elements the microstructure is composed of large ferritic grains. However, martensite blocks were observed. This could not have been predicted from the classical Fe-Cr binary phase diagram. On the contrary, when yttrium oxides are added with or without titanium, the microstructure is bimodal (or multimodal) with large grains and ultrafine grains. This bimodal microstructure is currently observed on ODS ferritic steels consolidated by hot isostatic pressing [20,40-41]. However, dilatometric and calorimetric tests show a partial austenitization for **WTi** and **LS** materials during heating but no martensitic blocks were observed by SEM. According to Brachet et al. and Lambard [19,42], the critical cooling rate to form a fully martensitic structure drastically decreases when nanometric precipitates are added into the microstructure.

Table 2 shows that the average nanoparticles size does not decrease significantly when the volume fraction of Y_2O_3 changes. Only the volume fraction of particles increases with yttria content. In 2002, Ukai et al. studied the precipitation evolution of Fe-12Cr-2W steels re-inforced by several content of yttria and titanium (0.13%Ti – 0.13% Y_2O_3 and 0.22%Ti – 0.22% Y_2O_3) [43]. They observed an increasing volume fraction. However, the average diameter of nanoparticles decreases slightly to ~ 1 nm. Thus, present microstructural observations are in good agreements with these previous studies.

Furthermore, as it is well known, the grain size evolves with the volume fraction of nanoparticles [13-14]. EBSD analyses highlighted an evolution of the grain size, and especially of the surface fraction of ultrafine grains, with the content of Y_2O_3 . Refinement of grain size was observed when the volume fraction of nanoparticles increases. Coarsening of nanometric grains is limited probably due to grain boundaries pinning by nanoparticles during the elaboration steps. Cayron et al. have demonstrated the same precipitation effect on the evolution of grain size [44]. Cayron et al. showed that the microstructure of an EUROFER steel consolidated by HIP and strengthened with 0.2% Y_2O_3 contains 40% nanometric grains whereas the value increases to 70% for a HIPed EUROFER steel containing 1% of yttria [44]. This was also observed by Hoelzer et al [45]. Using *in situ* analyses by X-ray diffraction at Synchrotron Soleil, Boulmat et al. noticed a coarsening of grains as well as a reduction of dislocation

density during heat treatment usually used after HIP [16]. It corresponds to a dynamic recrystallization phenomenon. According to Sallez et al. [15], this phenomenon is limited by the content of nano-oxides due to an increase of the Zener pressure.

4.3. *Effect of grain size*

A variation of the critical cooling rate to achieve full martensitic structure was observed on the calorimetric measurements between **WTi** and **LS** ferritic steels. Indeed, material without titanium is 100% ferritic with a furnace shutted off cooling whereas the **LS** material exhibits a martensitic transformation for the same cooling condition. The microstructure of the **LS** steel is fully ferritic when the cooling rate is lower or equal to 0.2°C/s.

Danon et al. [46] have shown the appearance of two populations of prior austenite grains in an ODS EUROFER 97 steel. After austenitization, the microstructure of this low activation martensitic steel is bimodal. Danon et al. highlight the fact that austenite is firstly formed on small grains before extending on the coarser prior austenitic grains [46]. Brachet et al. [19] give a relationship between grain size and martensitic critical cooling rate (Fig. 11). Thus, the prior austenite grain size is supposed to be equivalent to the average nanometric grain size. Using the study of Brachet et al. [19] and EBSD analyses, the critical cooling rate could be estimated. **WTi** material presents an average nanometric grain size of 260 nm whereas it is 410 nm for the **LS** material. Using extrapolation of the Fig. 11, the critical cooling rate below which austenite is transformed into ferrite is about 1700°C/h (or 0.47°C/s) and 1150°C/h (or 0.32°C/s) respectively for the **WTi** and **LS** alloys. A very good agreement with dilatometric measurements is thus observed. It indicates that the variation of the phase transformation kinetics and martensite occurrence or not are mainly due to the differences of the ultrafine prior-austenitic grain sizes.

5. **CONCLUSIONS**

In the present work, the effect of chemical composition of Fe-14Cr ODS steels consolidated by hot isostatic pressing has been investigated. Microstructural characterizations have been carried out on each material. The main conclusions are:

- The un-strengthened steel is composed of large grains and martensite blocks whereas ODS ferritic steels have a bimodal microstructure with large and nanometric grains.
- **Ref** material is homogeneous whereas segregation of W and Cr were observed on other materials.

- Chemical heterogeneities correspond to ultrafine grains and martensite blocks.
- Fe-14Cr steels with a low (or zero) content of titanium exhibits a $\alpha \rightarrow \alpha + \gamma$ phase transformation upon heating whereas **Ref** material is always fully ferritic.
- Phase diagram depends on carbon content in solid solution and thus titanium content forming stable carbides up to high temperatures. The lowest titanium content in solid solution is around 0.1 wt% to prevent chemical partitioning phenomenon.
- Microstructural parameters, such as nanoparticles size, volume fraction and grain size, influence the value of the martensitic critical cooling rate in accordance with previous studies.

Acknowledgements

The program MACNA funded in tripartite agreement between CEA, AREVA and EDF supported this study. The authors would like to acknowledge Françoise Barcelo (CEA Saclay) for the EBSD analyses. The LTMEx laboratory (CEA Saclay) is warmly acknowledged for the elaboration of model materials.

References

- [1] G.R. Odette, M.J. Alinger, B.D. Wirth: Recent developments in irradiation-resistant steels, *Ann. Rev. Mater. Res.* 38 (2008) 471-503.
- [2] P. Yvon, F. Carré, Structural materials challenge for advanced reactor systems, *J. Nucl. Mater.* 385 (2009) 217-222.
- [3] P. Dubuisson, Y. De Carlan, V. Garat, M. Blat, ODS ferritic/martensitic alloys for Sodium Fast Reactor fuel pin cladding, *J. Nucl. Mater.* 428 (2012) 6-12.
- [4] M.J. Alinger, G.R. Odette, D.T. Hoelzer, On the role of alloy composition and processing parameters in nanocluster formation and dispersion strengthening in nanostructured ferritic alloys, *Acta Mater.* 57 (2009) 392-406.
- [5] C.A. Williams, P. Unifantowicz, N. Baluc, G.D.W. Smith, E.A. Marquis, The formation and evolution of oxide particles in oxide-dispersion-strengthened ferritic steels during processing, *Acta Mater.* 61 (2013) 2219-2235.
- [6] A. Deschamps, F. De Geuser, J. Malaplate, D. Sornin, When do oxide precipitates form during consolidation of oxide dispersion strengthened steels?, *J. Nucl. Mater.* 482 (2016) 83-87.
- [7] P. Unifantowicz, Z. Oksiuta, P. Olier, Y. De Carlan, N. Baluc, Microstructure and mechanical properties of an ODS RAF steel fabricated by hot extrusion or hot isostatic pressing, *Fusion Eng. Des.* 86 (2011) 2413-2416.
- [8] Z. Oksiuta, P. Hosemann, S.C. Vogel, N. Baluc, Microstructure examination of Fe-14Cr ODS ferritic steels produced through different processing routes, *J. Nucl. Mater.* 451 (2014) 320-327.
- [9] X. Boulnat, D. Fabrègue, M. Perez, M.H. Mathon, Y. De Carlan, High-temperature tensile properties of nano-oxide dispersion strengthened ferritic steels produced by mechanical alloying and spark plasma sintering, *Metall. Mater. Trans. A* 44 (2013) 2461-2465.
- [10] H. Zhang, Y. Huang, H. Ning, C.A. Williams, A.J. London, K. Dawson, Z. Hong, M.J. Gorley, C.R.M. Grovenor, G.J. Tatlock, S.G. Roberts, M.J. Reece, H. Yan, P.S. Grant, Processing and microstructure characterization of oxide dispersion strengthened Fe-14Cr-0.4Ti-0.25Y₂O₃ ferritic steels fabricated by spark plasma sintering, *J. Nucl. Mater.* 464 (2015) 61-68.
- [11] I. Hilger, X. Boulnat, J. Hoffmann, C. Testani, F. Bergner, Y. De Carlan, F. Ferraro, A. Ulbricht, Fabrication and characterization of oxide dispersion strengthened (ODS) 14Cr steels consolidated by means of hot isostatic pressing, hot extrusion and sparks plasma sintering, *J. Nucl. Mater.* 472 (2016) 206-214.
- [12] M. Dadé, J. Malaplate, J. Garnier, F. De Geuser, N. Lochet, A. Deschamps, Influence of consolidation methods on the recrystallization kinetics of a Fe-14Cr based ODS steel, *J. Nucl. Mater.* 472 (2016) 143-152.

- [13] M. Dadé, J. Malaplate, J. Garnier, F. De Geuser, F. Barcelo, P. Wident, A. Deschamps, Influence of microstructural parameters on the mechanical properties of oxide dispersion strengthened Fe-14Cr steels, *Acta Mater.* 127 (2017) 165-177.
- [14] P. Dou, A. Kimura, R. Kasada, T. Okuda, M. Inoue, S. Ukai, S. Ohnuki, T. Fujisawa, F. Abe, Effects of titanium concentration and tungsten addition on the nano-mesoscopic structure of high-Cr oxide dispersion strengthened (ODS) ferritic steels, *J. Nucl. Mater.* 442 (2013) 95-100.
- [15] N. Sallez, P. Donnadieu, E. Courtois-Manara, D. Chassaing, C. Kübel, F. Delabrouille, M. Blat-Yrieix, Y. Bréchet, On ball-milled ODS ferritic steel recrystallization: from as-milled powder particles to consolidated state, *J. Mater. Sci.* 50 (2015) 2202-2217.
- [16] X. Boulmat, N. Sallez, M. Dadé, A. Borbély, J.L. Béchade, Y. De Carlan, J. Malaplate, Y. Bréchet, F. De Geuser, A. Deschamps, P. Donnadieu, D. Fabrègue, M. Perez, Influence of oxide volume fraction on abnormal growth of nanostructured ferritic steels during non-isothermal treatments: an in situ study, *Acta Mater.* 97 (2015) 124-130.
- [17] B. Al-Mangour, *Powder metallurgy of stainless steel: state-of-the art, challenges, and development*, eds. A. Pramanik and A.K. Basak (Nova Science Publishers, New York, 2015) 37-80.
- [18] A. Alamo, J.C. Brachet, A. Castaing, C. Lepoittevin, F. Barcelo, Physical metallurgy and mechanical behavior of FeCrWTaV low activation martensitic steels: Effects of chemical composition, *J. Nucl. Mater.* 258-263 (1998) 1228-1235.
- [19] J.C. Brachet, V. Lambard, A. Alamo, Studies of phase transformations occurring in conventional, low activation (LA) and oxide dispersion strengthened (ODS) 7-11%Cr-(Mo, W, V, Nb, Ta) martensitic steels, *Proceedings of the International Conference on Solid-Solid Phase Transformations '99* (1999) 1609-1612.
- [20] M.A. Auger, T. Leguey, A. Muñoz, M.A. Monge, V. De Castro, P. Fernández, G. Garcés, R. Pareja, Microstructure and mechanical properties of ultrafine-grained Fe-14Cr and ODS Fe-14Cr model alloys, *J. Nucl. Mater.* 417 (2011) 213-216.
- [21] A. Kimura, H.S. Cho, N. Toda, R. Kasada, K. Yutani, H. Kishimoto, N. Iwata, S. Ukai, M. Fujiwara, High burnup fuel cladding materials R&D for advanced nuclear systems: Nano-sized oxide dispersion strengthened steels, *J. Nucl. Sci. Technol.* 44 (2007) 232-328.
- [22] A. Karch, Études des évolutions microstructurales lors de la transformation à chaud d'aciers ferritiques renforcés par dispersion d'oxydes, PhD thesis, Ecole Nationale Supérieure des Mines de Paris, 2014.
- [23] A. Steckmeyer, M. Praud, B. Fournier, J. Malaplate, J. Garnier, J.L. Béchade, I. Tournié A. Tancray, A. Bougault, P. Bonnaille, Tensile properties and deformation mechanisms of a 14Cr ODS ferritic steel, *J. Nucl. Mater.* 405 (2010) 95-100.
- [24] J.H. Kim, T.S. Byun, D.T. Hoelzer, S.W. Kim, B.H. Lee, Temperature dependence of strengthening mechanisms in the nanostructured ferritic alloy 14YWT: Part I – Mechanical and microstructural observations, *Mater. Sci. Eng. A* 559 (2013) 101-110.
- [25] H. Oka, T. Tanno, S. Ohtsuka, Y. Yano, T. Uwaba, T. Kaito, M. Ohnuma, Effect of thermo-mechanical treatments on nano-structure of 9Cr-ODS steel, *Nucl. Mater. Energy* 9 (2016) 346-352.
- [26] D. Sornin, P.F. Giroux, E. Rigal, D. Fabregue, R. Soulas, D. Hamon, Influence of powder outgassing conditions on the chemical, microstructural, and mechanical properties of a 14 wt% Cr ferritic ODS steel, *Metall. Mater. Trans. A* 48 (2017) 5559-5566.
- [27] K. Ara, Magnetic characteristics of ferromagnetic stainless steels, *IEEE Trans. Magn.* 25 (1989) 2617-2623.
- [28] P. Dobis, J. Bruestlova, M. Bartlova, Curie temperature in ferromagnetic materials and visualized magnetic domains, *3rd International Symposium for Engineering Education* (2010) Ireland.
- [29] T. Shrestha, S.F. Alsagabi, I. Charit, G.P. Potirniche, M.V. Glazoff, Effect of heat treatment on microstructure and hardness of grade 91 steel, *Metals* 5 (2015) 131-149.
- [30] H. Sakasegawa, L. Chaffron, F. Legendre, L. Boulanger, T. Cozzika, M. Brocq, Y. De Carlan, Correlation between chemical composition and size of very small particles in MA957 ODS ferritic alloy, *J. Nucl. Mater.* 384 (2009) 115-118.
- [31] P.J. Cunat, Aciers inoxydables – Critères de choix et structure, *Techniques de l'Ingénieur* (mars 2000).
- [32] P. Olier, J. Malaplate, M.H. Mathon, D. Nunes, D. Hamon, L. Toualbi, Y. De Carlan, L. Chaffron, Chemical and microstructural evolution of ODS Fe-14CrWTi steel during manufacturing stages, *J. Nucl. Mater.* 428 (2012) 40-46.
- [33] T. Okuda, S. Nomura, N. Nakanishi, M. Fujiwara, H. Takahashi, Development of oxide dispersion strengthened (ODS) ferritic alloys with excellent high temperature creep strength and neutron irradiation resistance, *Proc. 1st Japan International SAMPE* (1989) 1616-1621.

- [34] I.S. Kim, B.Y. Choi, C.Y. Kang, T. Okuda, P.J. Maziasz, K. Miyahara, Effect of Ti and W on the mechanical properties and microstructure of 12% Cr base mechanical-alloyed nano-sized ODS ferritic alloys, *ISIJ International* 43 (2003) 1640-1646.
- [35] M. Ratti, D. Leuvrey, M.H. Mathon, Y. De Carlan, Influence of titanium on nano-cluster (Y-Ti-O) stability in ODS ferritic materials, *J. Nucl. Mater.* 386-388 (2006) 540-543.
- [36] P. Franke, H.J. Seifert, *Ternary system Cr-Fe-W*, eds Ternary steel systems: Phase diagrams and phase transition data (Springer, Berlin, 2012) 419-429.
- [37] Z. Amy, Caractérisation de l'acier inoxydable X5CrNi18-10 et étude de son oxydation à température, PhD thesis, Université Mouloud NAMMERE de Tizi-ouzou, 2013.
- [38] P. He, On the structure-property correlation and the evolution of nanofeatures in 12-13.5% Cr oxide dispersion strengthened ferritic steels, PhD thesis, Karlsruhe Institut für Technologie, 2013.
- [39] Q. Zhao, Z. Ma, L. Yu, H. Li, Z. Wang, Y. Liu, Inhibition effect of Ti on the formation of martensite lath in 14Cr oxide dispersion strengthened steel, *Metals* 8 (2018) 1-17.
- [40] Z. Oksiuta, N. Baluc, Microstructure and Charpy impact properties of 12-14Cr oxide dispersion-strengthened ferritic steels, *J. Nucl. Mater.* 374 (2008) 178-184.
- [41] Z. Oksiuta, A. Ozieblo, K. Perkowski, M. Osuchowski, M. Lewandowska, Influence of HIP pressure on tensile properties of a 14Cr ODS ferritic steel, *Fusion Eng. Des.* 89 (2014) 137-141
- [42] V. Lambard, Développement d'une nouvelle nuance martensitique ODS pour l'utilisation sous rayonnement à haute température, PhD thesis, Université Paris Sud UFR scientifique d'Orsay, 2000.
- [43] S. Ukai, T. Okuda, M. Fujiwara, T. Kobayashi, S. Mizuta, H. Nakashima, Characterization of high temperature creep properties in recrystallized 12Cr-ODS steel claddings, *J. Nucl. Sci. & Tech.* 39 (2002) 872-879.
- [44] C. Cayron, E. Rath, I. Chu, S. Launois, Microstructural evolution of Y_2O_3 and $MgAl_2O_4$ ODS EUROFER steels during their elaboration by mechanical milling and hot isostatic pressing, *J. Nucl. Mater.* 335 (2004), 83-102.
- [45] D.T. Hoelzer, J. Bentley, M.A. Sokolov, M.K. Miller, G.R. Odette, M.J. Alinger, Influence of particle dispersions on the high-temperature strength of ferritic alloys, *J. Nucl. Mater.* 367-370 (2007) 166-172.
- [46] C.A. Danon, T. Guilbert, J.C. Brachet, Kinetics of the austenite-ferrite isothermal phase transformation in 9 % Cr low activation martensitic steels, *Proceeding of International Conference of New Developments on Metallurgy and Applications of High Strength Steels* (2008).

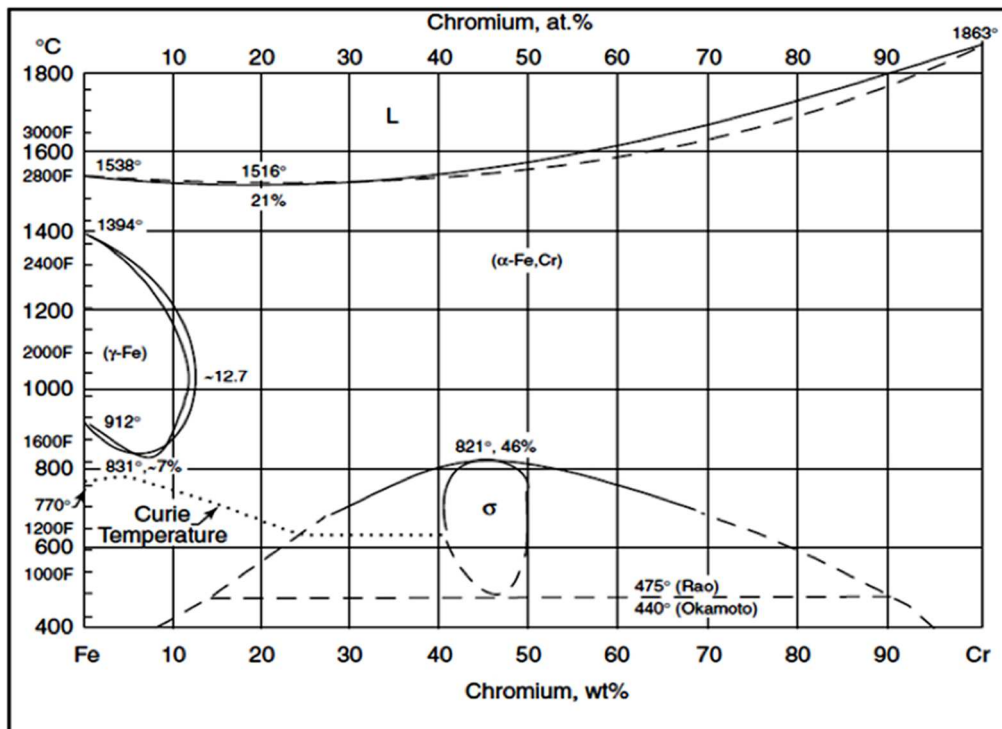


Fig. 1. Fe-Cr diagram [17].

Table 1. Main elements chemical composition data (wt%) for the different ferritic steels.

	Cr	W	Ti	Y	C
US	13.78 $\pm 0.25\%$	1.00 $\pm 0.25\%$	-	-	0.012 $\pm 0.001\%$
LS	14.25 $\pm 0.25\%$	1.06 $\pm 0.03\%$	0.08 $\pm 0.01\%$	0.06 $\pm 0.01\%$	0.045 $\pm 0.003\%$
WTi	14.23 $\pm 0.25\%$	1.09 $\pm 0.03\%$	-	0.20 $\pm 0.04\%$	0.029 $\pm 0.002\%$
Ref	14.51 $\pm 0.25\%$	0.93 $\pm 0.02\%$	0.22 $\pm 0.01\%$	0.16 $\pm 0.01\%$	0.028 $\pm 0.002\%$

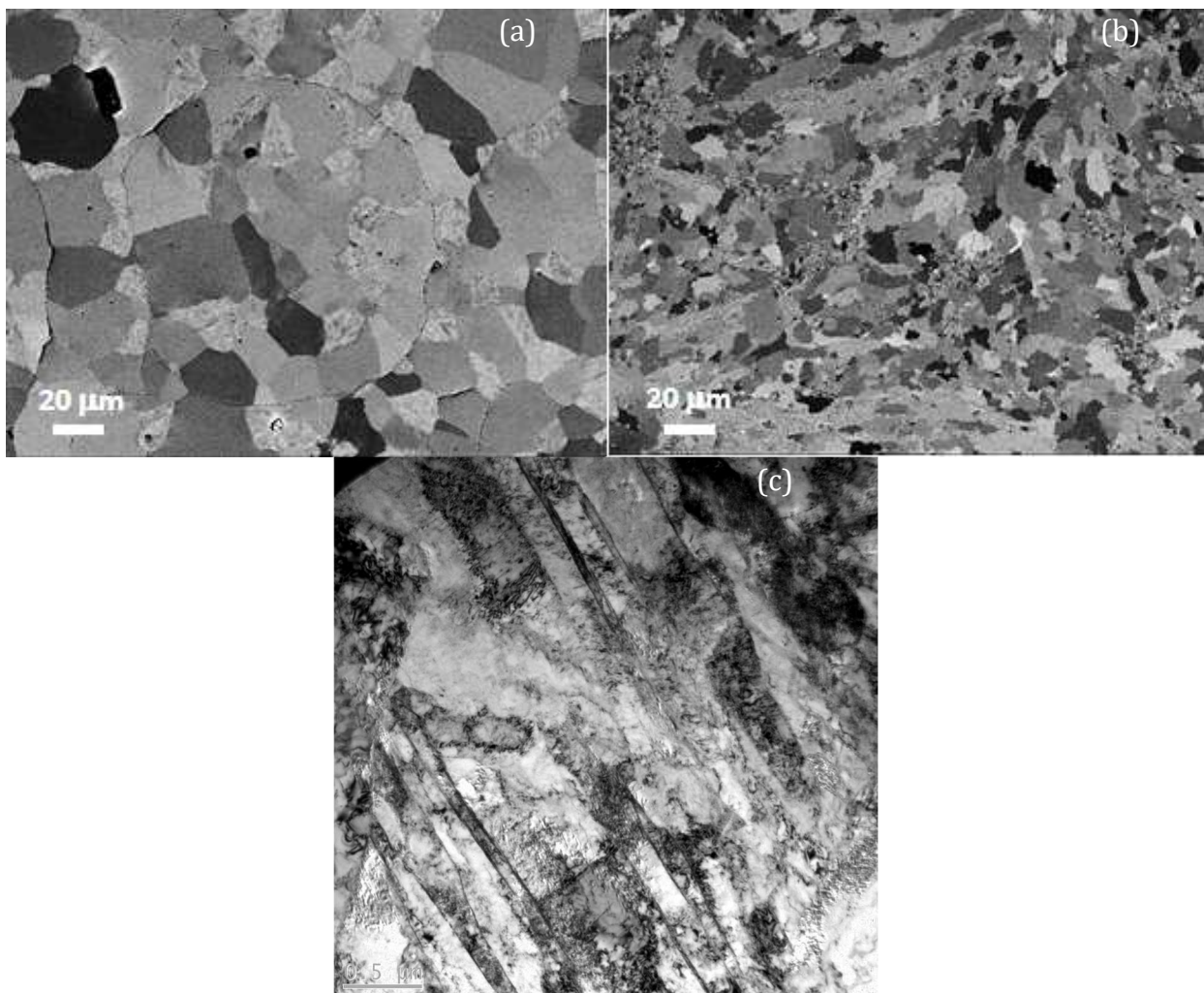


Fig. 2. SEM micrographs of the un-strengthened (a) and the reference (b) materials and TEM micrograph of the **US** material showing the martensitic microstructure (c).

Table 2. Average grain size, surface fraction of small grains/martensite blocks and precipitation state of the four ferritic steels.

	US	LS	WTi	Ref
--	-----------	-----------	------------	------------

Mean grain size (μm)	27.6	4.3	9.0	6.5
Surface fraction of small grains/martensite blocks (%)	14.4	30.4	23.2	21.4
Average particles size (nm)	-	1.6	2.6	1.3
Volume fraction of particles (%)	-	0.31	0.46	0.52

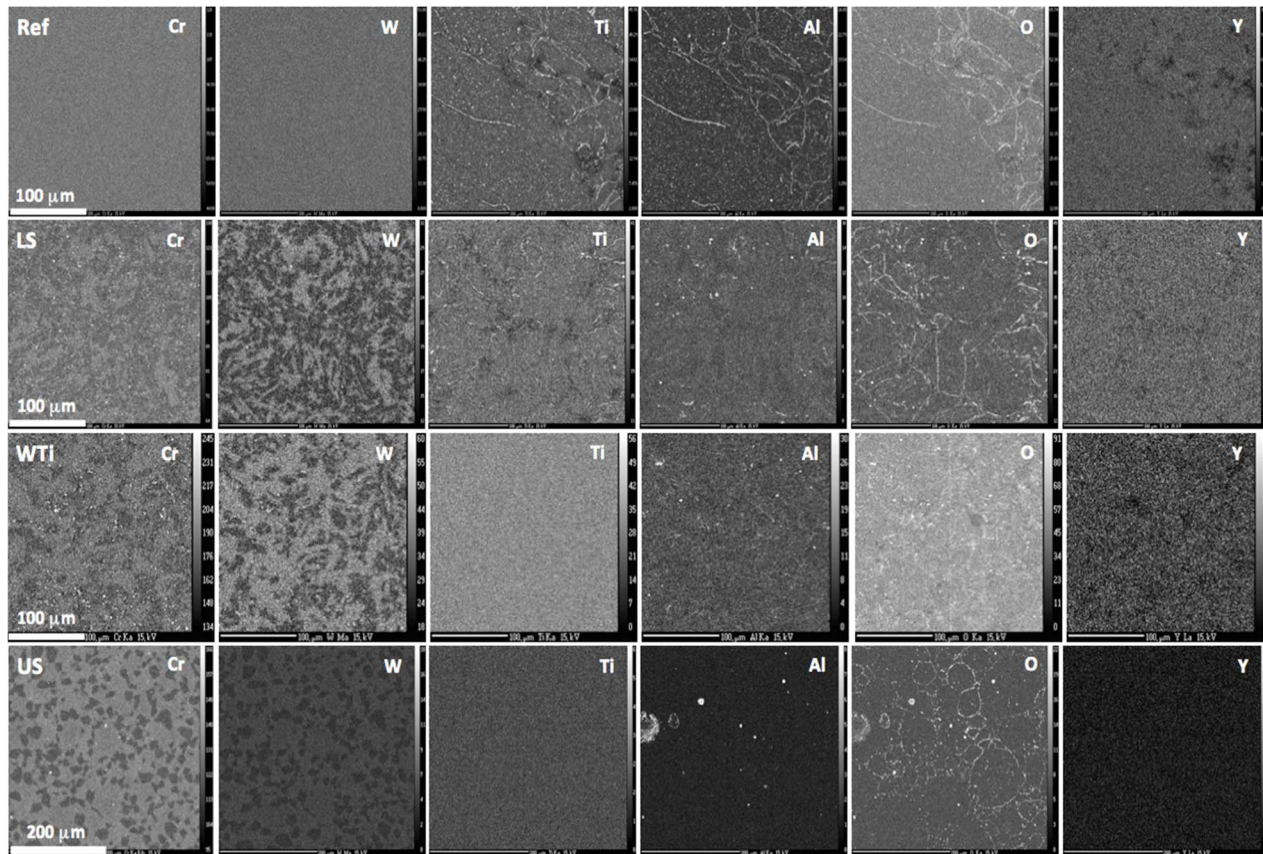


Fig. 3. EPMA concentration maps showing the distribution of Cr, W, Ti, Al, O and Y for each material.

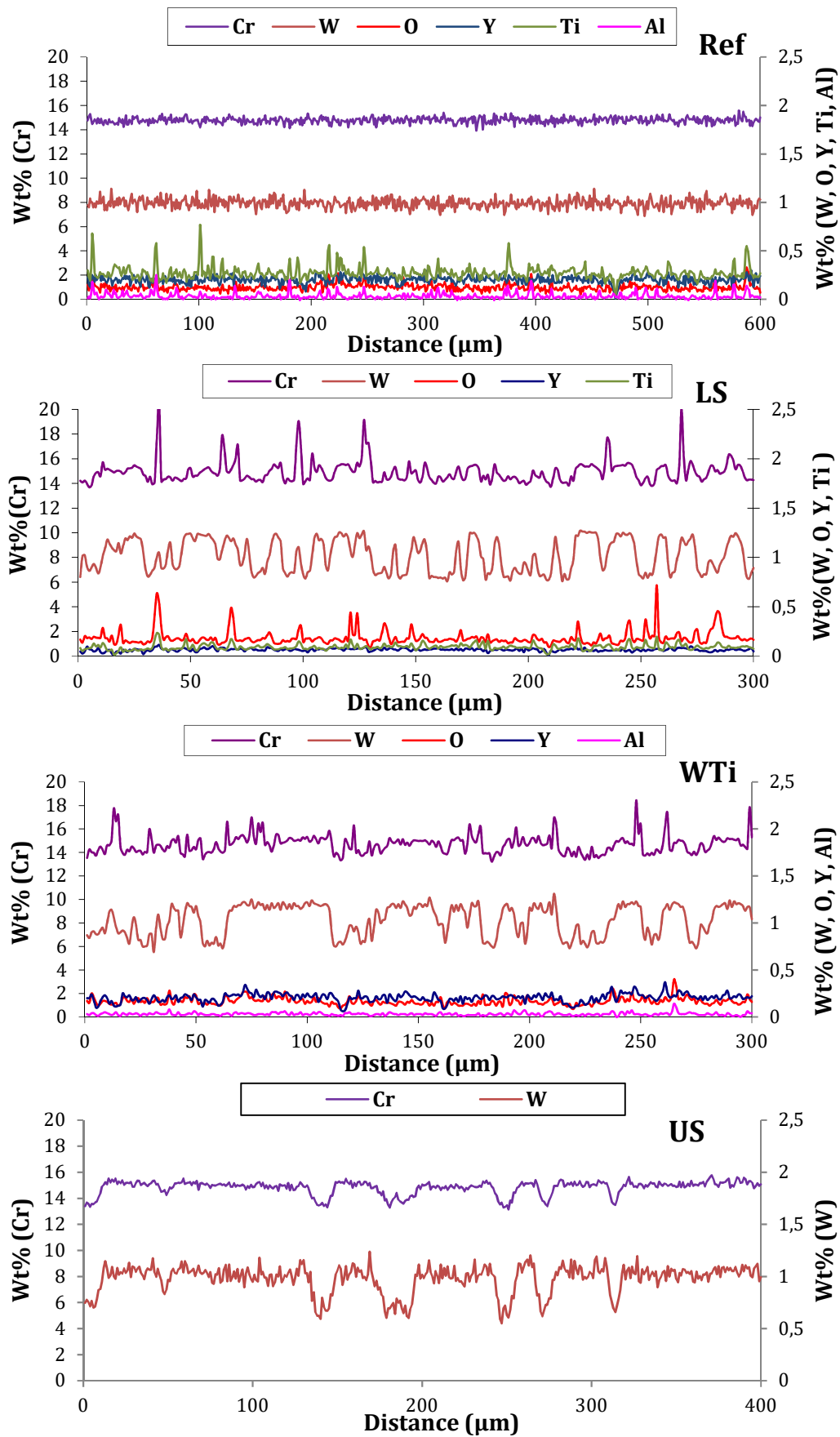


Fig. 4. Quantitative analyses (weight%) of the principal chemical elements. The filiations have been realized using an acquisition step of 1 μm. (For interpretation of the references to color in this figure legend, the reader is referred to the web version of this article).

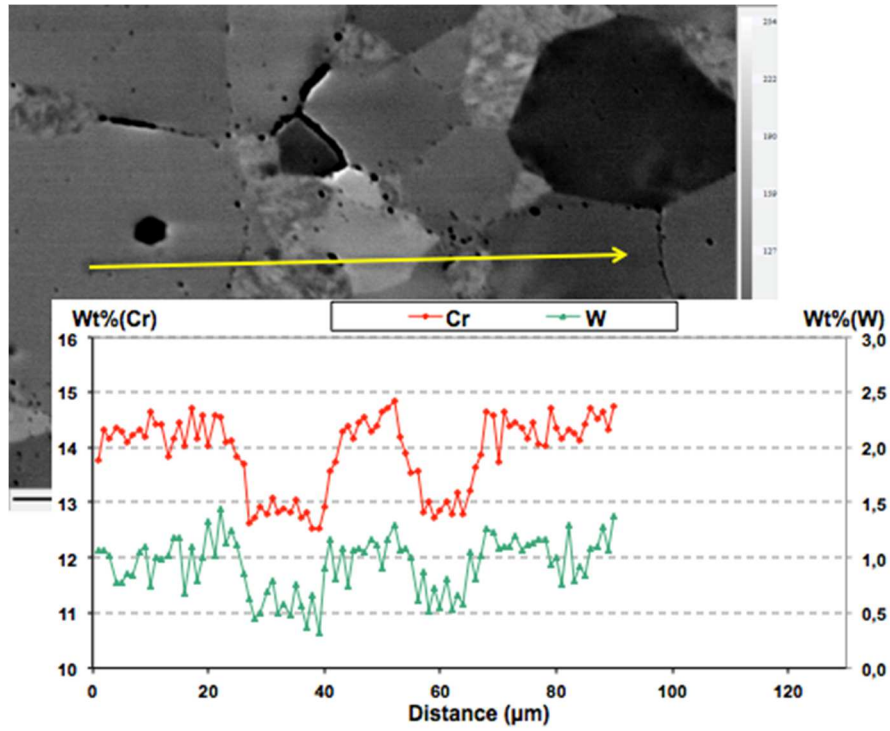


Fig. 5. Quantitative filiation on the un-strengthened ferritic steel US. The acquisition step is 1 µm. (For interpretation of the references to color in this figure legend, the reader is referred to the web version of this article).

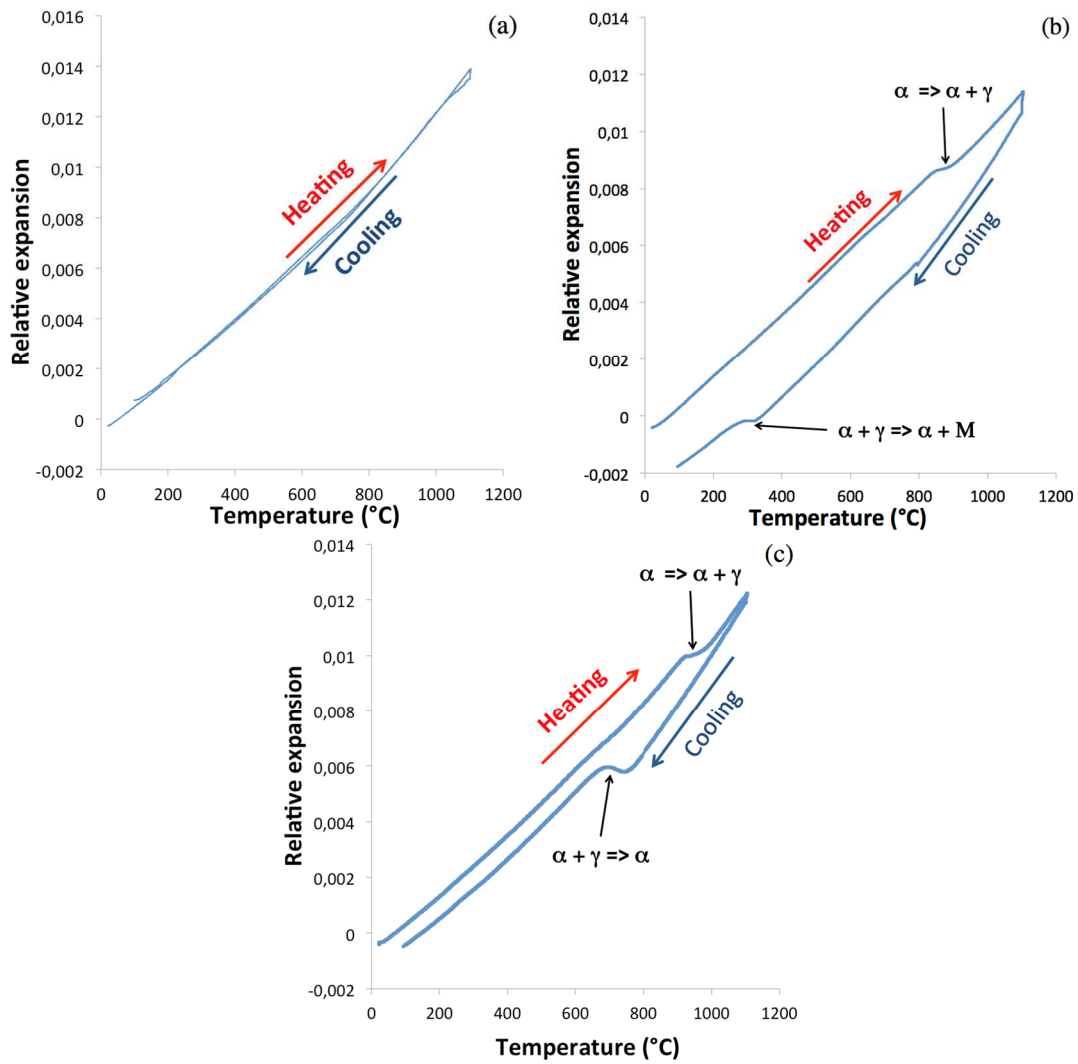


Fig. 6. Dilatometric curves from room temperature to 1100°C for the **Ref** material (a), the ferritic steel un-strengthened (b) and the **LS** material (c). Dilatometric tests have been carried on **US** and **LS** materials with a heating rate of 10°C/s and a cooling rate close to the HIP conditions ($V_c = 0.2^\circ\text{C}/\text{s}$) whereas a high cooling rate ($V_c = 100^\circ\text{C}/\text{s}$) was used for the **Ref** material.

Table 3. Enthalpy values determined with DSC curves and estimation of the austenite content.

	Fe-9%Cr	US	LS	WTi
Enthalpy ΔH (J/g)	10 [28]	1.5	3.9	2.8
Austenite content	100%	15%	39%	28%

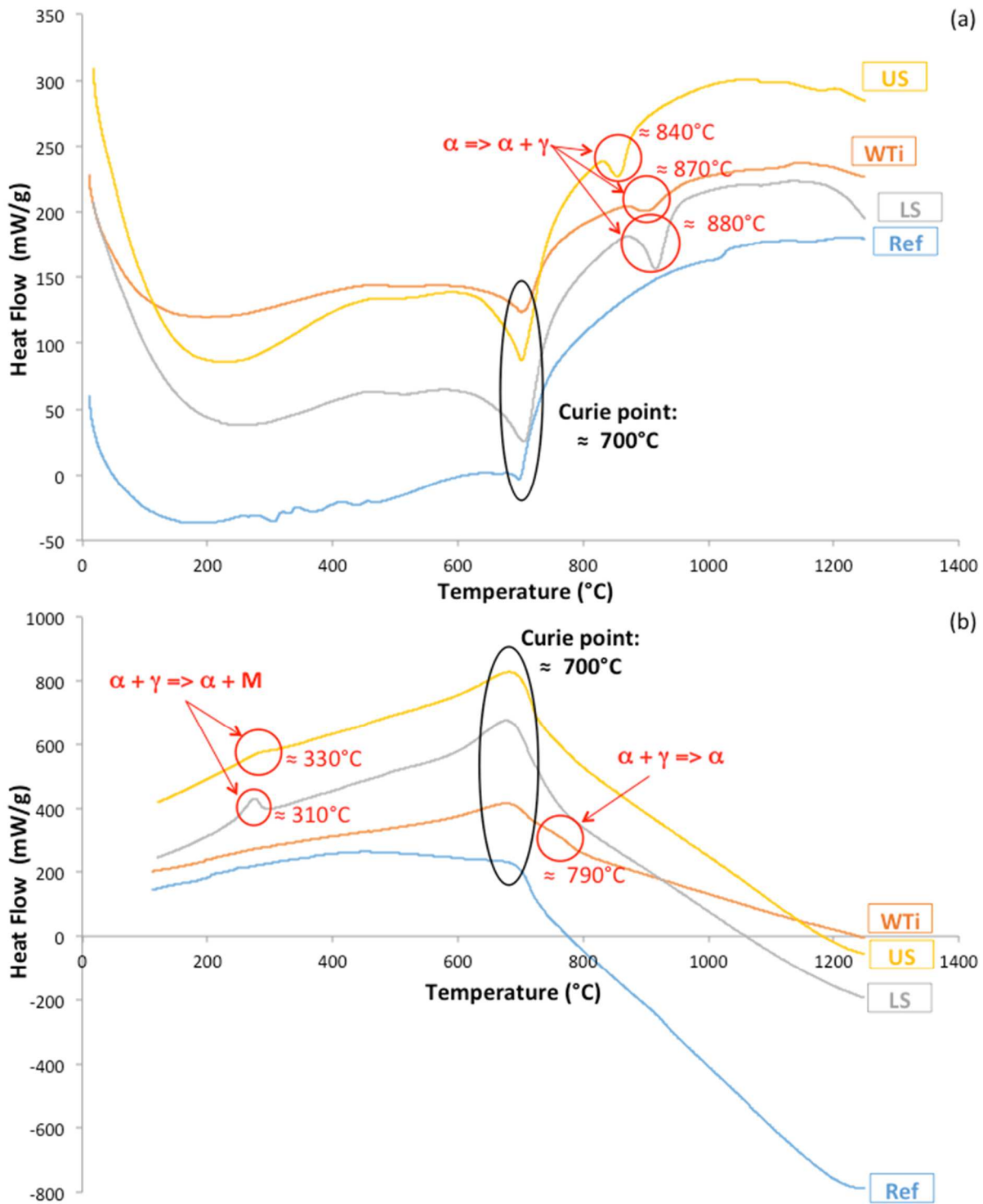


Fig. 7. DSC curves of ferritic steels **Ref**, **LS**, **WTi** and **US** at heating rate of $10^{\circ}\text{C}/\text{min}$ (a) and cooling with a furnace shutted off (b).

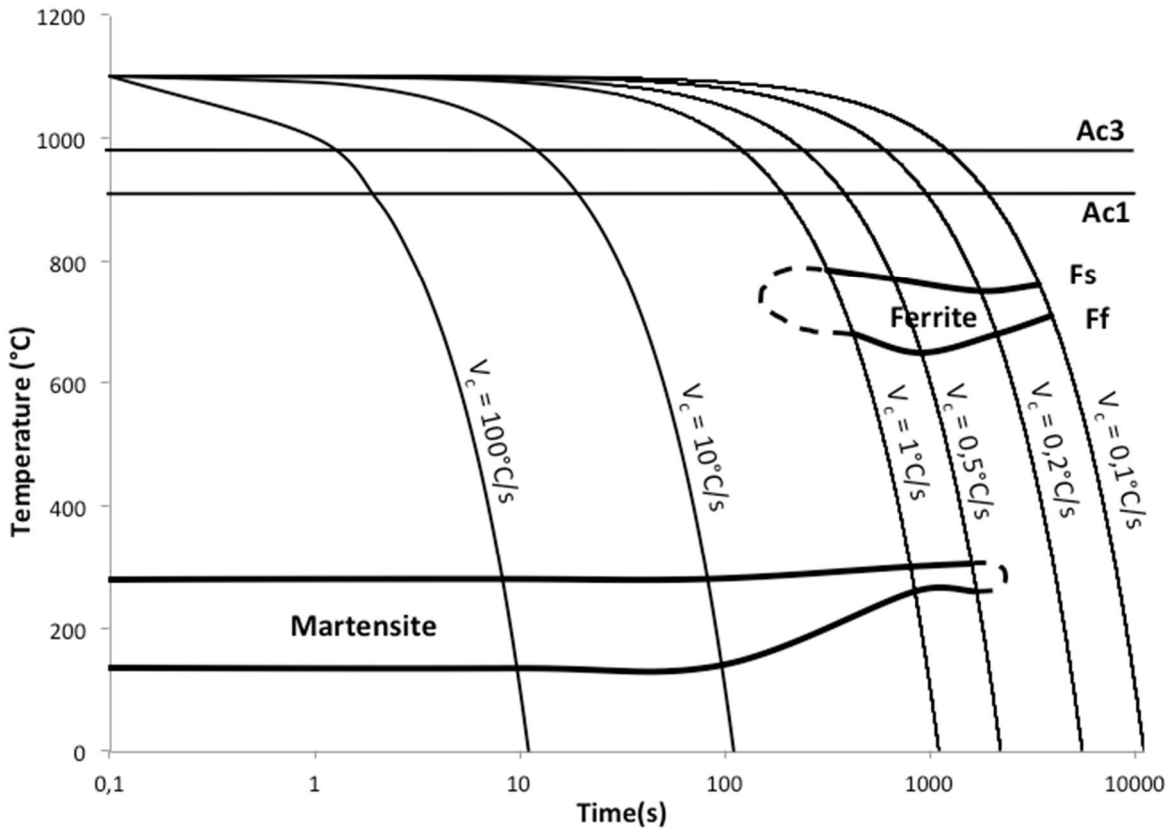


Fig. 8. CCT diagram of the ODS ferritic steel **WTi**. Samples were heated at 1100°C for 1 min.

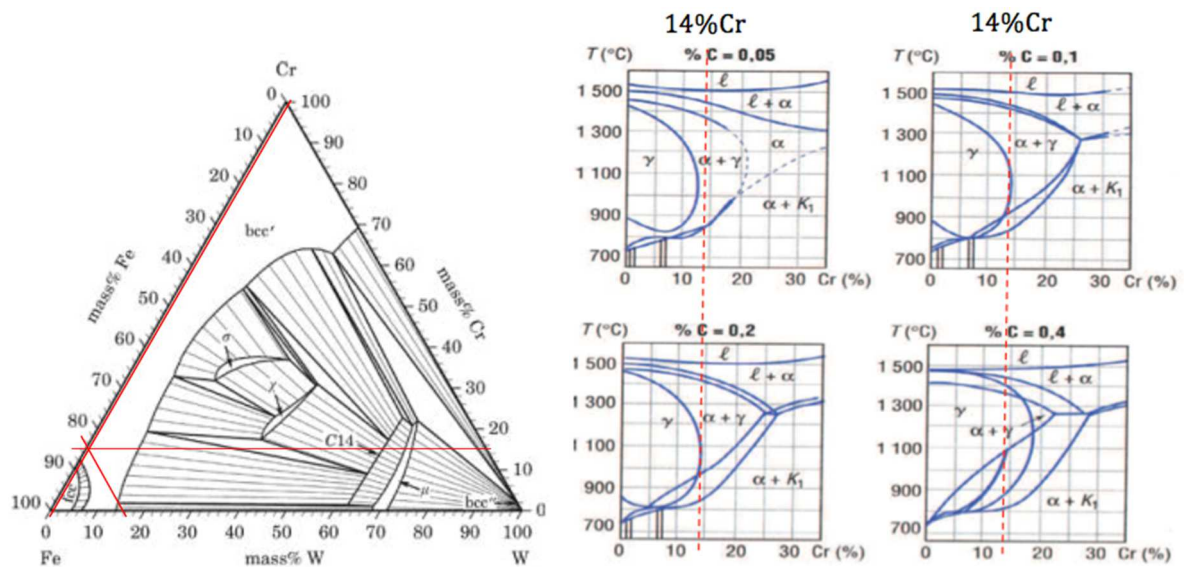


Fig. 9. (a) Ternary Diagram Fe-Cr-W at 1100°C [36]. The red lines correspond to the nominal concentration of a ferritic steel Fe-14Cr-1W and allow to determine the crystalline structure after HIP process. (b) Pseudo-binary diagram Fe-Cr with different carbon content [37].

Table 4. Quantitative analyses of gammagene elements (Ni, N, C and Mn) for each ferritic steel.

	wt% Ni	wt% N	wt% C	wt% Mn
US	0.21	0.03	0.01	0.30
LS	0.21	0.11	0.05	0.28
WTi	0.21	0.07	0.03	0.28
Ref	0.22	0.04	0.03	0.28

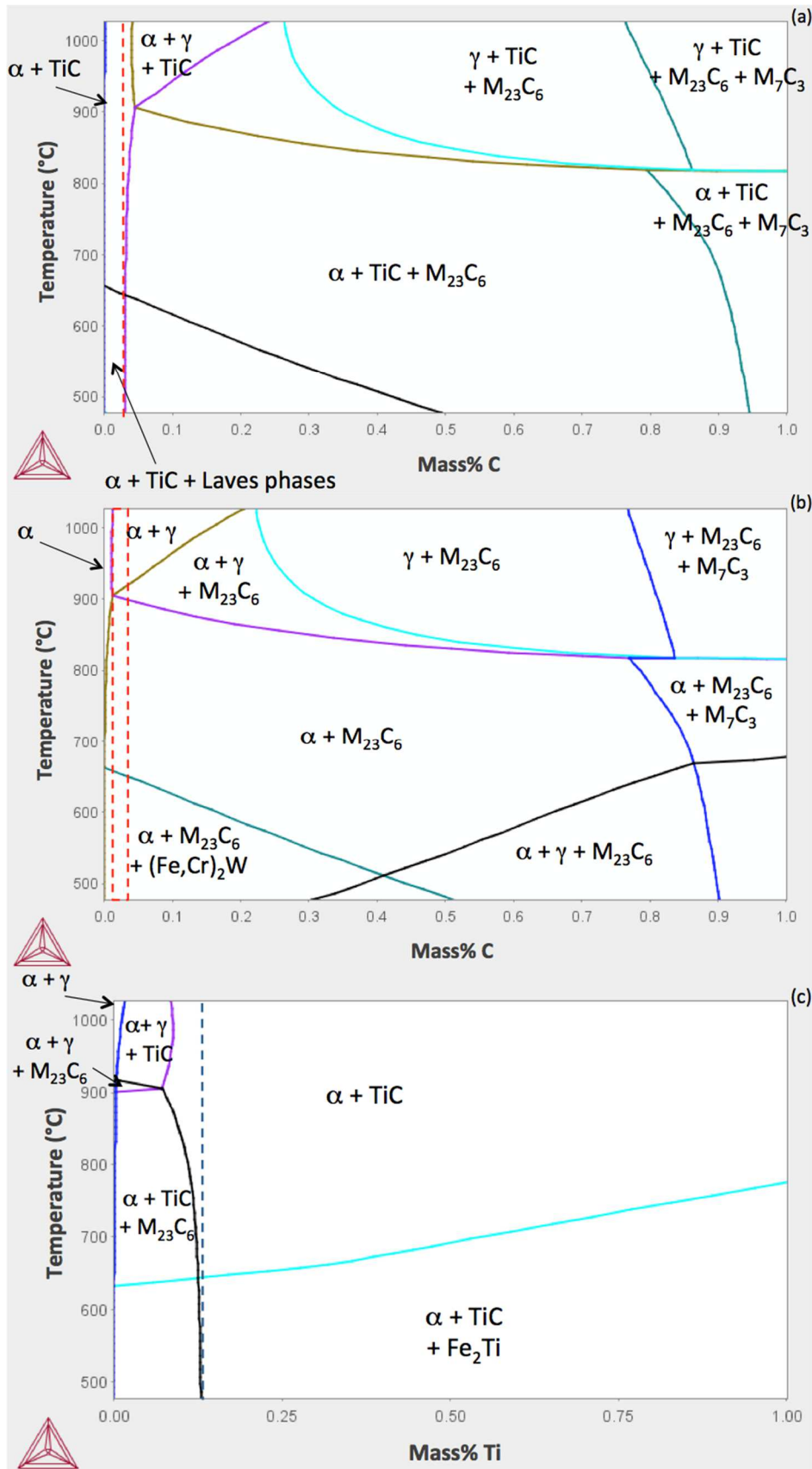


Fig. 3. Pseudo-binary phase diagram Fe-C of the **Ref** material with the carbon content illustrated by the red dashed line (a). Pseudo-binary phase diagram Fe-C of a Fe-14Cr-1W ferritic steel with the carbon content of **WTi** and **LS** ferritic steels in red dashed line (b). Pseudo-binary diagram Fe-Ti of a Fe-14Cr-1W-0.3C steel with the titanium content of **Ref** materials not trapped into nanometric oxides Y-Ti-O and illustrated by blue dashed line (c). All pseudo-binary phase diagrams have been calculated with ThermoCalc software.

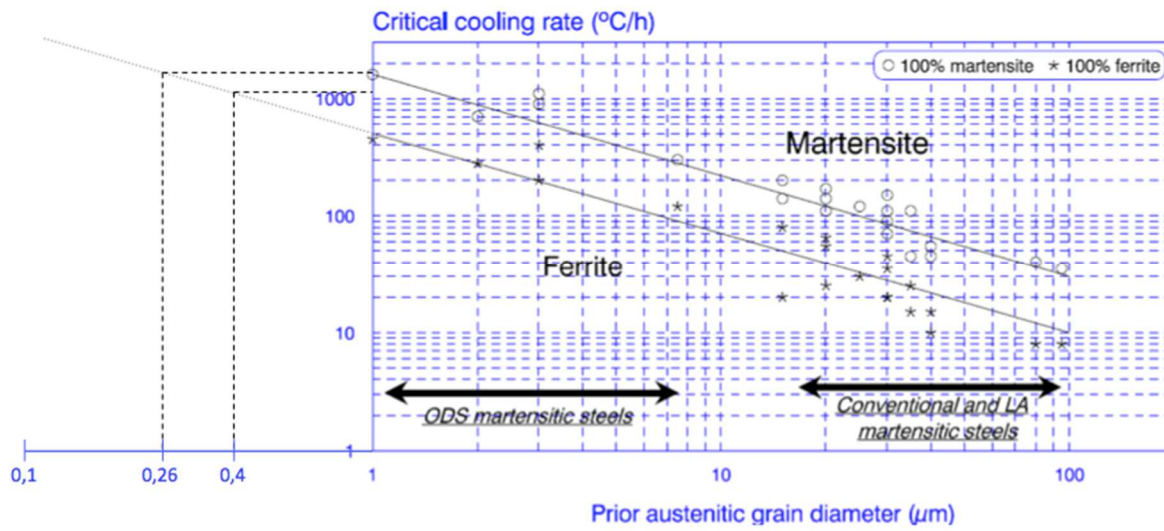


Fig. 4. Critical cooling rate values depending on the prior austenite grain size [19].